Railway Engineering Science
https://doi.org/10.1007/s40534-026-00447-2

In-service surface temperature measurement of tread braked wheels with a novel on-board infrared rugged device

G. Megna[1] · A. Bracciali[2] · A. Francesconi[2]

Received: 6 February 2026 / Revised: 25 May 2026 / Accepted: 28 May 2026

Abstract
Temperatures reached on railway wheels tread during braking with composite blocks are responsible for extensive damage unknown when cast iron brake blocks were used. The accurate measurement of wheel tread temperature during braking becomes then fundamental to tune models to estimate thermomechanical damage due to the combined thermal and vertical/longitudinal actions at the wheel/rail contact especially in fully loaded conditions. This measurement is not trivial during service braking, as contact (sliding) thermocouples are not reliable in the long term and conventional infrared sensors in the wavelength range 8–14 µm are not suitable for bright steel surfaces. Moreover, thermal cameras with the correct parameters are expensive and too delicate to be installed even temporarily on a freight wagon bogie frame. A low-cost, non-contact measuring device based on a rugged single-spot pyrometer sensitive to the correct infrared emission wavelength (1.5–1.8 µm) was developed. The pyrometer is mounted on a motorized slider continuously spanning the tread surface for a practically unlimited time. The functionality of a prototype was checked during braking sessions on a homologated brake rig, tuning the actual wheel tread emissivity with the help of specific finite element thermal simulations. The device was then mounted on a Y25 bogie and in-service measurements were performed. The paper describes the development and calibration of the device, concluding with the results of the in-service tests.

Keywords Tread braking · Freight wagons · Thermal loads · Pyrometer · Infrared sensor · Braking tests

1 Introduction

Temperature measurements of the wheel tread surface of freight wagons during the application of block braking may be performed using measuring systems based on:

- *Embedded thermocouples*, inserted into holes drilled in the bottom of wheel rim, usually 5–10 mm below the tread surface;
- *Sliding thermocouples*, i.e., thermocouples touching the wheel tread with a given elastic preload;
- *Thermal cameras,* by which the infrared radiation of an object is converted in temperature and displayed as images.

All these sensors are commonly used on brake rigs whose main scope is to test braking systems (brake disks, brake pads, brake blocks, and low-stress tread braked wheels) for homologation purposes. Nevertheless, they show strong limitations when installed on-board a railway vehicle for long-term monitoring of the wheel tread temperature in service.

Thermocouples embedded below the running surface do not measure its actual temperature and require a complex and expensive telemetry system; moreover, holes drilled in the rim are not safe and therefore they are not allowed in service. Sliding thermocouples directly measure the wheel surface temperature and are inexpensive, but they are not sufficiently rugged for long-lasting tests and their output is strongly affected by airflow, friction, and vibrations. Thermal cameras are expensive (~ 100 k€) when the specific radiation wavelength range is requested (see below) and they would hardly survive the harsh conditions found under a freight wagon in service.

A survey about the temperature measuring systems and the related results available in literature can be found in [1]. While several applications can be found for bench tests,

✉ G. Megna
gianluca.megna@ing.unipi.it

[1] Department of Industrial and Civil Engineering, University of Pisa, 56122 Pisa, Italy

[2] Department of Industrial Engineering, University of Florence, 50139 Florence, Italy

in-service applications are much rarer. A thermal camera placed wayside to measure the mean temperature of the side of the wheel rim of passing freight trains is used in [2], while sliding thermocouples applied on the wheel surface of freight trains and passenger vehicles are described in [3–5]. In-service measurements using embedded thermocouple up to 2.5 mm below the wheel surface were found only in [6].

Trackside infrared temperature detectors, known as hot axle box detectors (HABD), installed on the railway lines every 20–30 km, are commonly used to detect a fault condition of axle's bearings, giving alarms for temperatures over a defined limit value. They are sometimes equipped (Fig. 1) with additional sensors for the measurements of the temperature of braking components (brake disks or the internal side of the wheels in case of tread brakes). A threshold of 250 °C is typically set for wheels. These devices were used for the extensive monitoring of tread braked ([7, 8]). It should be noted that HABD measure the temperature at the lateral (internal) side of the wheel and not the wheel tread temperature; moreover, the measured surfaces are characterized by a blackish/opaque aspect that leads to an infrared emission spectrum much different from that of a bright wheel tread.

The literature review of in-service measurements showed that maximum temperature values are relatively dispersed and that there is not a consensus about them. This is also due to the intrinsic difficulty in keeping all the parameters under control during line tests. The lowest values (below 100 °C) are reported in [8], while the highest values (over 600 °C) when tests without dynamic braking from locomotives were performed are shown in [7]. More recently average wheel temperatures of passing trains below 240 °C were measured [2]. However, all these tests cannot be directly related to the temperatures reached on the running surface of the wheels due to the limitations of the measuring systems.

Bench tests can be easily controlled, and exceptional continuous braking loads can be safely simulated. Tread temperatures up to 600 °C are commonly measured, but during these tests, the actual in-service conditions are not reproduced, the major lack being the absence of the wheel–rail contact. Counter roller may reasonably reproduce wheel-rail radial loads, but the *rail-chill* effect is too far from the one encountered when rolling on an infinitely long and cold rail, making data from test rigs not fully reliable.

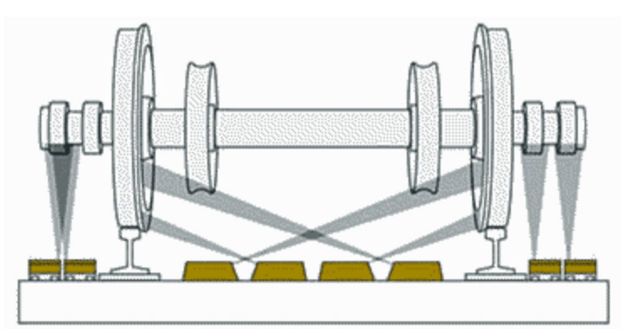

Fig. 1 Infrared measuring detector for bearings, brake disks, and wheels (adapted from [9])

To overcome the limitations of the existing devices, a new rugged and low-cost contactless device based on an infrared spot pyrometer with specific characteristics was developed to continuously collect data during service.

Compared to thermal cameras, spot pyrometers have the advantage to be available in the short wavelength infrared range at limited costs. To the authors' knowledge, the first and only application of pyrometer in railway is dated 1948 [10] in which a lead sulfide pyrometer ($\lambda = 1$–3 μm) was used during bench tests braking. No other references were found even if in 1972, the ORE B64-RP10 [11] suggested the use of pyrometer in the short wavelength infrared range (SWIR) $\lambda = 0.7$–1.6 μm for the wheel surface temperature measurement. However, in the other industrial fields dealing with metals, the use of SWIR pyrometers is quite common and several references can be found [12].

2 Basics of infrared temperature measurements

Infrared thermal radiation ranges from about 0.8 μm to 1 mm, although the useful range for temperature measurements ends at around 15 μm. The range 0.8–15 μm is usually called the *thermal infrared range*. The greatest difficulty in the use of infrared detectors consists in determining the correct emission parameters (wavelength of emission and emissivity coefficient).

The *Planck radiation law* describes the black body radiation i_b as a function of the absolute temperature T and the wavelength λ [13]. It is often used in its equivalent form (Eq. (1)) considering the constants c_1 and c_2 (known as the *first and second radiation constants*, $c_1 = 3.74 \times 10^{-16}$ Wm^2 and $c_2 = 14{,}388$ μmK) [14].

$$i_\mathrm{b}(\lambda, T) = c_1 \left[\lambda^5 \left(\mathrm{e}^{\frac{c_2}{\lambda T}} - 1\right)\right]^{-1}. \tag{1}$$

The *black body radiation* (Fig. 2a) exhibits a maximum at a wavelength that depends on the temperature according to the *Wien displacement law* (Eq. (2)), where h is the Planck's constant, c is the speed of light, k is the Boltzmann's constant. The maximum value shifts toward shorter wavelengths when temperature increases.

$$\lambda_\mathrm{m} = \frac{hc}{4.965kT} = \frac{2898}{T}. \tag{2}$$

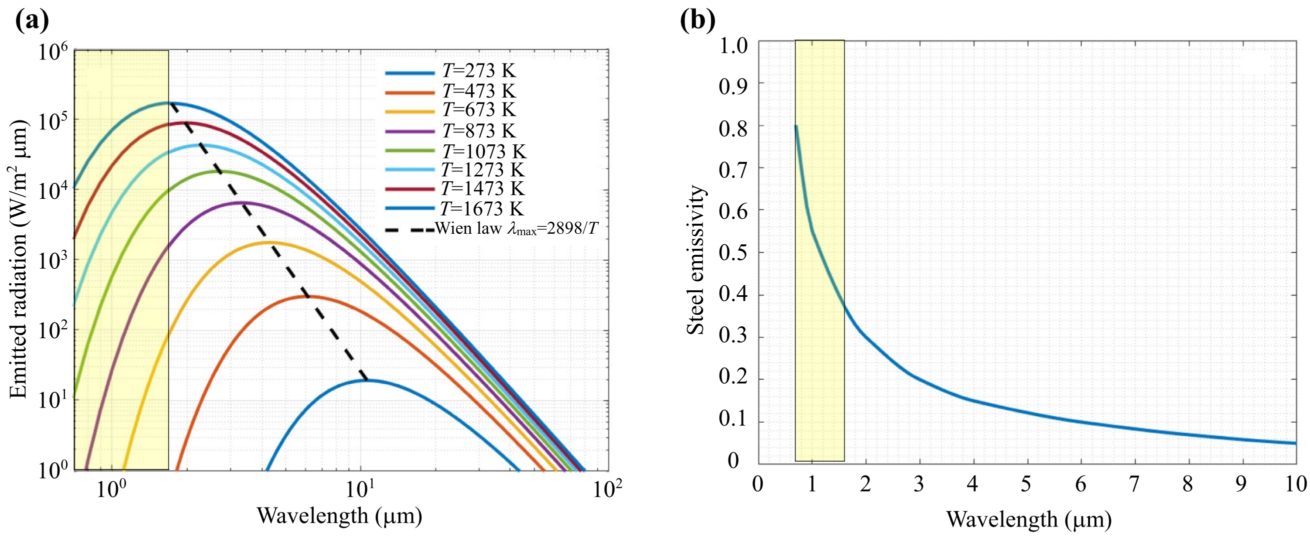

Fig. 2 **a** Black body radiation according to the Planck radiation law. The curve maxima, described by Wien displacement law, are joined by a dashed line. The lowest curve, at $T=273$ K (0 °C), is maximum at $\lambda=10$ μm. **b** Typical emissivity of steel as a function of wavelength (modified from [14]). The tinted box shows the short wavelength infrared range (SWIR) $\lambda=0.7$–1.6 μm

The radiation emitted by a real object is always smaller than that of a black body by a factor called *emissivity coefficient* or simply *emissivity* ε. If the emissivity is the same for all wavelengths the body is called *gray body*; otherwise, it is called *selective body* if ε varies with the wavelength.

The emissivity depends on the material, the conditions of its surface, its temperature, and the wavelength. Polished steel and metals such as the surface of railway wheels and rails in contact are in general selective bodies (as oxidized or damaged surfaces will alter this), and their emissivity is very low for wavelengths $\lambda>2$ μm (Fig. 2b). Therefore, "*for metallic materials, the shortest possible wavelength should be used, as the measuring error increases in correlation to the wavelength*" [14].

The response $S(T)$ of a thermal detector to black body radiation is obtained integrating Eq. (1) over all wavelengths (from 0 to ∞) according to Eq. (3), where $s(\lambda)$ is spectral sensitivity of the thermal detector and C is a constant depending on its optical and geometrical characteristics [15].

$$S(T) = C\int_{0}^{\infty} s(\lambda)i_{\mathrm{b}}(\lambda, T)\mathrm{d}\lambda. \tag{3}$$

Considering the finite bandwidth of the wavelength range, i.e., the mean wavelength λ_{c} and the bandwidth $\Delta\lambda$ of the thermal detector, this function can be approximated using Eq. (4), where A and B are constant values.

$$S(T) \approx \left(\mathrm{e}^{\frac{c_2}{(AT+B)}} - 1\right)^{-1}. \tag{4}$$

If the bandwidth is sufficiently small ($\Delta\lambda\approx0$), it results $A\approx\lambda_{\mathrm{c}}$ and $B\approx0$ [15]. Under this hypothesis, the emissivity of a selective body can be considered independent from the wavelength, and the output of the thermal detector can be written as the sum of three contributions [15]:

$$\varepsilon_{\mathrm{m}}S(T_{\mathrm{m}}) = \varepsilon S(T_{\mathrm{t}}) + (1-\varepsilon)S(T_{\mathrm{w}}) + S(T_{\mathrm{d}}), \tag{5}$$

where T_{m} is temperature estimated by the thermal detector, ε_{m} is the emissivity defined in the thermal detector measuring chain (usually set initially to $\varepsilon_{\mathrm{m}}=1$), T_{t} is the real temperature of the object, T_{w} is temperature of the surroundings, and T_{d} is temperature of the detector. As T_{d} and T_{w} may be neglected when the object temperature is hot relative to surroundings and detector, the emissivity of the real body can be estimated as [16]

$$\varepsilon = \varepsilon_{\mathrm{m}}\left(\mathrm{e}^{\frac{c_2}{T_{\mathrm{t}}\lambda_{\mathrm{c}}}} - 1\right)\Big/\left(\mathrm{e}^{\frac{c_2}{T_{\mathrm{m}}\lambda_{\mathrm{c}}}} - 1\right). \tag{6}$$

The calibration of a measuring system based on a commercial infrared sensor is fundamental and may reveal a complex process. Infrared sensors are factory calibrated using black body radiators ($\varepsilon=1$), but this calibration is useless for measuring objects whose emissivity is unknown. Two-color pyrometers may be used to overcome the emissivity uncertainties, but while they work perfectly for gray bodies, large measuring errors appear if the two wavelengths are not properly chosen for selective bodies [17]. Black painting, a method often used to get a black body radiation emission, obviously cannot be applied on the wheel running surface,

The use of an infrared measuring system to measure wheel surface temperature requires therefore to calibrate its response by comparing its output with the temperatures measured with other methods of known accuracy and then adjusting its emissivity according to Eq. (6).

3 Development and calibration of the oscillating spot pyrometer measuring chain

3.1 Concept and prototype

Temperatures up to 500–600 °C are commonly reached on the wheel tread during tests on brake rigs. Infrared measurements with thermal cameras measuring the emission in the long-wave infrared range ($\lambda = 8$–14 μm) were found in literature [18, 19]. Detailed information about thermal cameras measuring characteristics are often not given in the papers found in literature, but it is reasonable to suppose that they are limited to the long-wave infrared range. According to the available literature, a mid-wave infrared range ($\lambda = 1.5$–5 μm) thermal camera was used only in [20] and in [21]. This is not a suitable sensor for the current type of testing because of lack of ruggedness (cryo-cooler with moving parts), glass optics (germanium lens), price (cooled systems are easily greater than ten times or more the currently used sensor), and filtering requirements for reasonable control over emissivity or even legal issues (dual-use technology). The application of thermal cameras is also often limited to bench tests and the only reference of in-service temperature measurement of brake disks with a long-wave infrared thermal camera is an unpublished paper [22].

As thermal cameras for short infrared wavelength ranges are expensive and delicate, a device incorporating a single-spot pyrometer DIAS DG 40N [23] was developed. Based on an indium gallium arsenide (InGaAs) detector with a fixed wavelength range ($\lambda = 1.5$–1.8 μm) centered on the maximum radiation emission of a bright steel surface, it has a large programmable temperature range and a programmable emissivity value. The available optics include a fixed lens focused on an optimal spot target of $d = 1.2$ mm at 210 mm, rejecting the components coming from off-spot sources. The pyrometer has no internal moving parts making it a perfect solution for the application under a freight wagon, offering the best compromise between performances and cost effectiveness.

The lower temperature bound of the pyrometer is 350 °C. This value was selected due to both the fact that not all short wavelength pyrometers are able to measure low temperatures (some models can arrive down to 250 °C) and that relevant reductions of mechanical properties of steel are expected only over 350–400 °C. A literature survey available in [1] has shown that yield stress is averagely reduced by about 20% at 400 °C and 60% at 600 °C. While it is possible that tread surface values could locally exceed 350 °C, in some cases, although limited to small zones, e.g., descending heavy haul or in the Gotthard descent braking, these are very specific that are very much not the norm.

An oscillating support with a motorized slideway was implemented to transversally scan the wheel tread by 80 mm, i.e., the standard width of a brake block. The full measuring cycle time (approximately 12 s) is compatible with the slow temperature changes of the tread surface. Faster changes of the wheel tread temperature, for example during stop braking, might be better detected easily reducing the cycle time if needed. In the present case, as the average behavior is of main interest, the temperature will be considered uniform along each circumference at a given time t.

The pyrometer was inserted in a *current loop* acquisition circuitry to measure the response between 4 and 20 mA, corresponding to a range of 350–1000 °C, using a 24-bit ADC acquisition module (NI 9219) driven by the National Instruments software installed on a laptop with Microsoft Windows OS. Figure 3a shows the configuration of the measuring system during the prototyping phase, while the connection scheme is detailed in Fig. 3b. The system

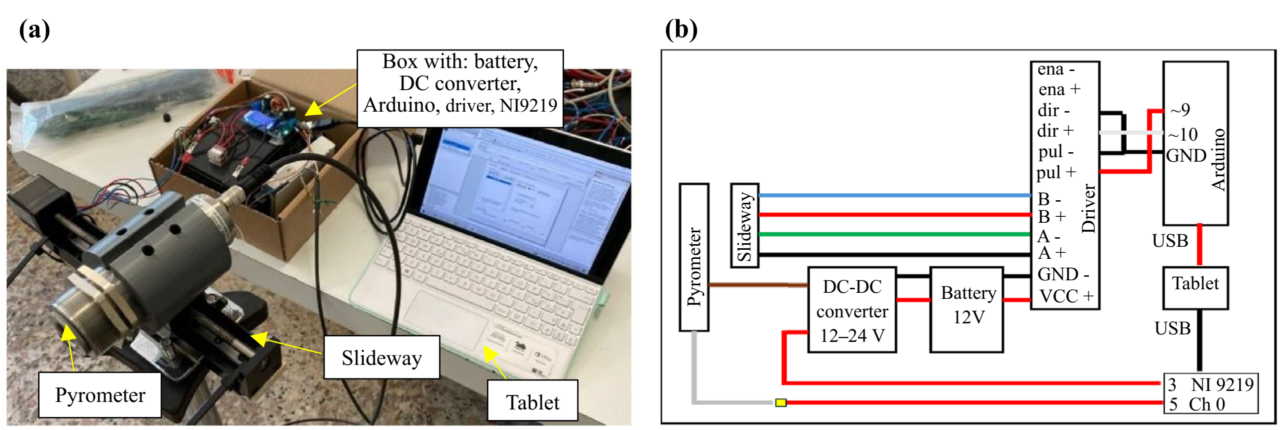

Fig. 3 **a** Arrangement of the measuring chain for the moving pyrometer with indication of the components and **b** their connection scheme

is compact and lightweight enough considering that only the pyrometer and the slideway are designed to be mounted on the bogie frame while the rest of the measuring system (power, control, and acquisition modules) will be housed on-board the "mothership" (wagon or locomotive) for continuous checking system operation and quality of the measurements.

3.2 Brake bench testing

The measuring system was calibrated during a braking test session on a UIC-homologated test bench (without counter-roller) consisting in a drag braking with a 2Bg braking configuration by using cast iron brake blocks that kept the surface clean through the entire test. Tests were attempted also with composite brake blocks without useful results as sintered brake blocks showed low wheel temperature values while organic brake blocks deposited block material on the tread making its surface opaque changing the emissivity. This last condition does not exist in service when the continuous wheel-rail contact "cleans" the tread. As said above, this is the most important limiting factor of conventional brake rigs about calibration of infrared emission sensors.

The wheel under testing was instrumented with three side-by-side sliding thermocouples spaced by 30 mm and three embedded thermocouples (5 mm below the tread) in the same lateral positions as the sliding thermocouples but installed on three sections at 120° around the wheel. The pyrometer under calibration was mounted at the prescribed distance (210 mm) from the wheel tread (Fig. 4). Pyrometer was sampled at 100 Hz, while thermocouples were sampled at 10 Hz.

The wheel speed was set to $v = 70$ km/h and a long drag braking was simulated by applying a braking power of about $P_{\mathrm{brake}} = 50$ kW (see details below). At the end of the braking phase, the wheel was kept rotating at only 3 km/h during the entire cooling phase to uniform the temperature distribution around the wheel tread surface avoiding uneven cooling due to airflow.

As the emissivity was unknown, its value was initially set to $\varepsilon = 1$. The maximum temperature values measured by the pyrometer and low-pass filtered at 10 Hz were close to 700 °C, greater than the values measured by the thermocouples (Fig. 5a and b). Noiser signal from the pyrometer may be explained considering the higher sampling frequency and the presence on the surface of hot bands and hot spots, as shown in Fig. 5c, which are "visible" by the pyrometer but not by thermocouples due to their thermal inertia.

Each thermocouple shows slower but relevant oscillations due to the unevenness of friction (and therefore of braking power) over time and over the contact length

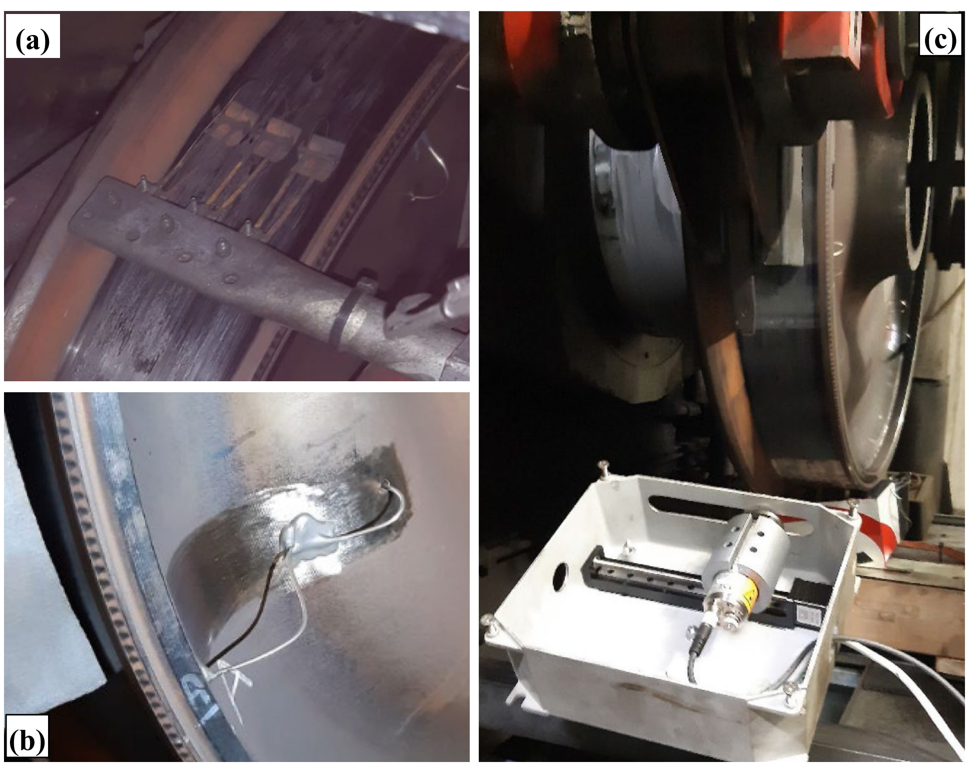

Fig. 4 Arrangement of the measuring devices on the test bench: **a** three side-by-side sliding thermocouples on the wheel tread spaced by 30 mm; **b** one of the three embedded thermocouples (installed at 120°); **c** the moving pyrometer in a metallic box at 210 mm from the wheel tread

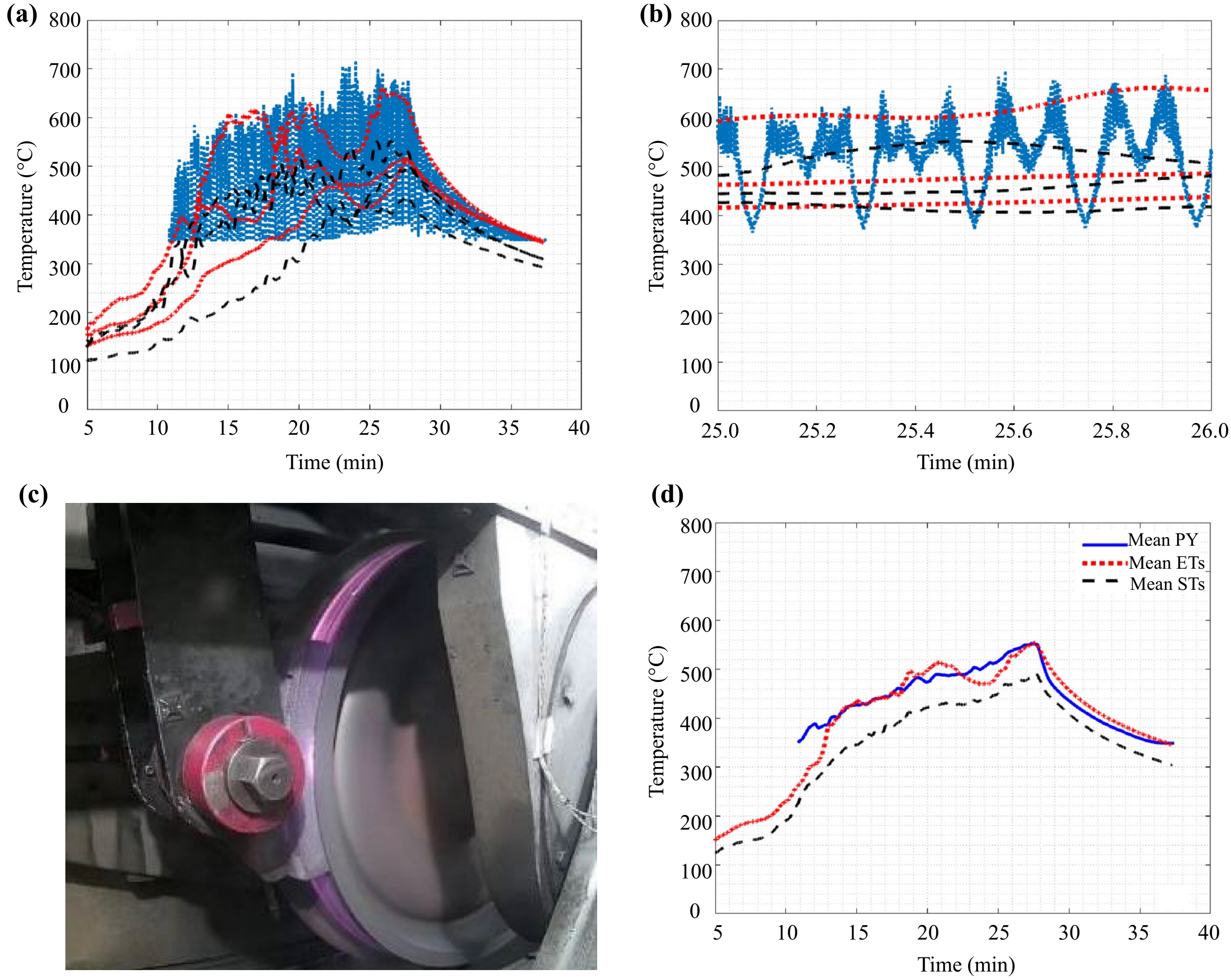

Fig. 5 **a** Temperature recorded by all measuring systems during braking tests with cast iron blocks (blue: pyrometer low-pass filtered at 10 Hz; red: three embedded thermocouples; black: three sliding thermocouples. **b** Detail of 1-min recording where the pyrometer runs are clearly visible. **c** Wheel under testing with visible hot bands during the heating phase. **d** Comparison of the mean surface temperature obtained with the three measuring methods (ET = embedded thermocouples, ST = sliding thermocouples, PY = pyrometer)

between brake block and wheel surface. Average values are more stable as shown in Fig. 5d. Data from the pyrometer were processed to obtain the mean temperature value of the wheel surface showing a good agreement with the average value of data from embedded thermocouples during both heating and cooling phases.

Probably due to a cooling effect of the airflow around the wheel tread while spinning, temperatures measured by the (calibrated) sliding thermocouples were lower (about 100 °C during braking and 50 °C during cooling) than those measured by embedded thermocouples, which contrasts with the physical evidence that the surface must be hotter than the tread volume at least during continuous braking application. Therefore, data from sliding thermocouples were not further used in the calibration process.

3.3 FE thermal model to estimate surface temperature

A simplified finite element model of the wheel thermal behavior was developed within ANSYS Workbench and

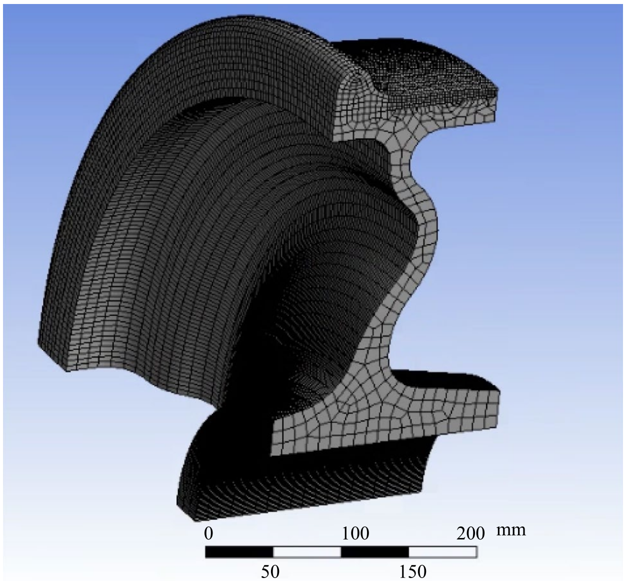

Fig. 6 Meshed model of the quarter wheel used to simulate the bench tests braking conditions

tuned on the data acquired by embedded thermocouples to estimate the actual surface temperature.

A 3D solid model of a quarter wheel was meshed with 58.667 eight nodes hexahedral thermal elements (Fig. 6) to perform transient simulations, assuming a static thermal power input uniformly distributed along the entire circumference of the wheel tread. Brake blocks were not modeled. Temperature dependent ER7 steel properties up to 800 °C were taken from [24] and [25].

The experimental input power was applied to the model as shown in Fig. 7a, considering that only part of the power generated at the braking interface flowed into the wheel. The amount of thermal power dissipated by cast iron brake blocks is defined in [24] as a function of the wheel diameter. For the given wheel ($d=771$ mm), it is about 20% of the braking power. Therefore, the power input applied to the wheel was the 80% of the total braking power. As commonly done for braking simulations [26], heat transfer between the wheel and the surroundings was modeled considering only convection.

To comply with the power applied during braking test, after an initial pre-heating ($t=0$–4 min), a two-stage heating phase on the wheel tread with $P_{brake}=12$ kW ($t=4$–8 min), and $P_{brake}=35$ kW ($t=11$–27 min) was applied. Between the two stages ($t=8$–11 min), the power was increased linearly. Then, the power input was removed ($t=27$–38 min) to simulate the cooling phase. During the braking phase, the following convection heat transfer coefficients were initially applied [24]:

- h=65 W/(m^{2}K) on the surfaces of the wheel web,
- h=56 W/(m^{2}K) on the surfaces of the rim and the flange,
- h=30 W/(m^{2}K) on the surfaces of the wheel tread.

The lower value on the wheel tread considers the presence of the brake blocks that were not modeled. To tune the cooling curve with the readouts of the embedded thermocouples, the convection heat transfer coefficients were gradually reduced during the cooling phase to consider the lower rotating speed of the wheel and that radiation may be more relevant if compared to the braking phase.

Due to the certainly uneven (and unknown) pressure distribution of the brake blocks on the wheel tread, the power input was considered applied non-uniformly on the tread. It was divided into three parallel areas to replicate the *banding* phenomenon often observed in practice [27] along the brake block width (80 mm) and adjusted as shown in Fig. 7b until the simulation results agreed with the embedded

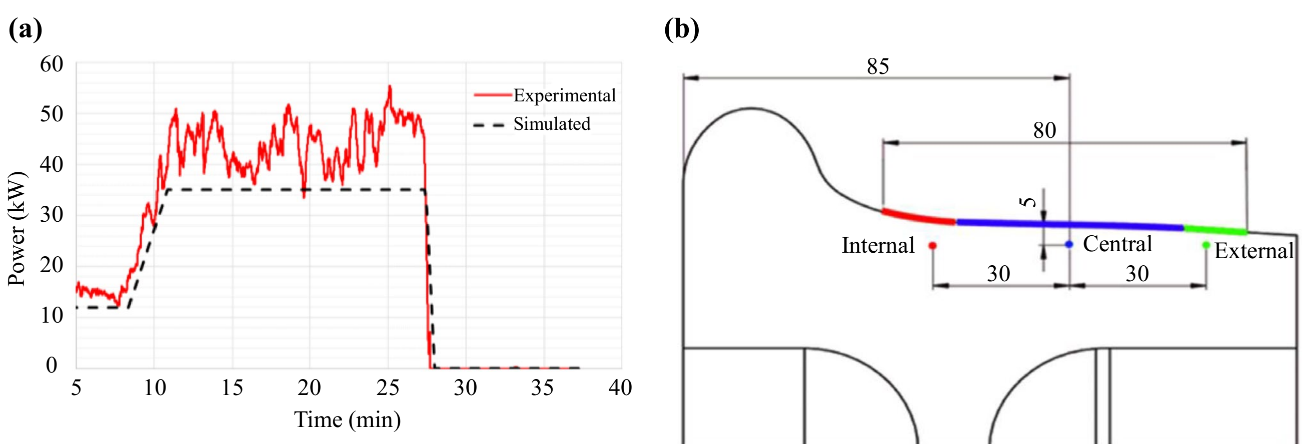

Fig. 7 **a** Measured and simulated power input applied to the model (approximately 80% of the braking power). **b** Wheel tread cross section with the three zones used for the power input application and the location of embedded thermocouples (unit: mm)

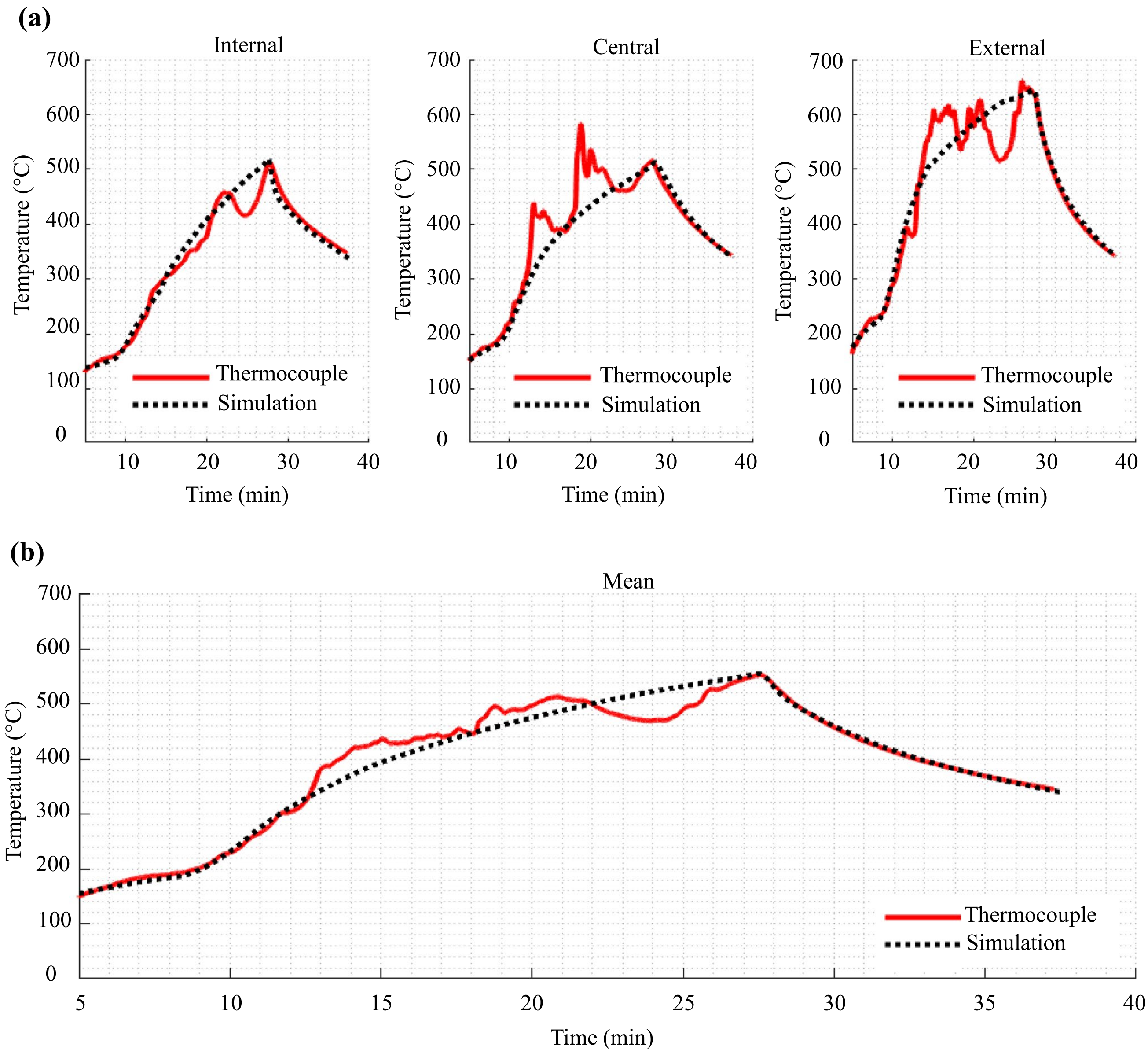

Fig. 8 Temperatures measured and simulated by **a** individual and **b** averaged embedded thermocouples

thermocouples readouts. Most of the braking power was applied to the external zone (50%), while the remaining power was applied to the internal zone (40%) and in the central zone (10%).

Figure 8 shows the individual and averaged data collected by embedded thermocouples (single and averaged values) compared to the values estimated at the corresponding nodes by the FE model. The irregular temperature measured by thermocouples, generated by the non-constant power input, is well fitted by the more regular simulation outputs. Both temperatures and gradients were correctly matched.

3.4 Estimation of the emissivity

Once the model was validated, data from the cooling phase were selected to estimate the emissivity of the surface to avoid the uncertainties related to both *banding* and hot spots present during brake application. Equation (6) was applied to simulate surface temperatures and pyrometer temperatures within the range $t = 28$–36 min. The resulting emissivity is shown in Fig. 9a, and its average value in the range $T = 370$–570 °C is $\varepsilon_{av} = 0.69$.

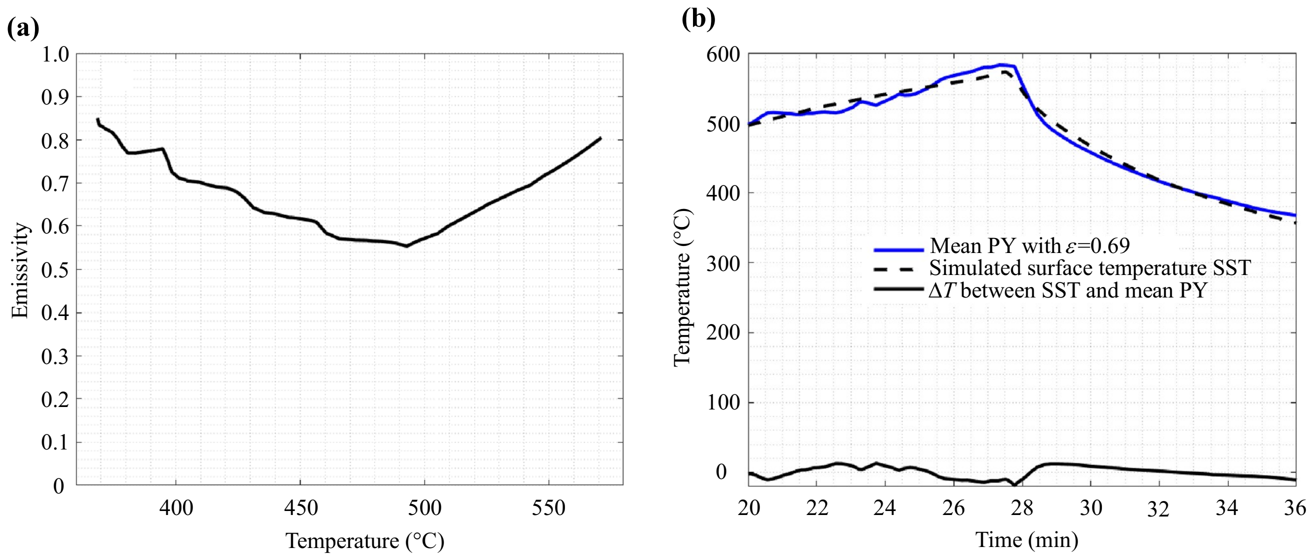

Fig. 9 **a** Emissivity $\varepsilon(T)$ calculated from Eq. (6). **b** Comparison of measured and estimated average surface temperatures simulated by considering a constant emissivity of $\varepsilon_{av} = 0.69$ and estimation error

Fig. 10 The test trainset

This emissivity value was applied to Eq. (4), i.e., $S(T_t) = S(T_m)/\varepsilon_{av}$, the temperature T_t was then calculated from Eq. (3) and compared to the simulated one (Fig. 9b) showing an error of ± 20 °C, which was considered acceptable seen the uncertainties intrinsic in the measuring and simulation processes.

4 In-service measurements

4.1 Installation of the measuring device

The prototype device was adapted to be mounted on the Y25 bogie frame of a freight wagon for in-service temperature measurements. A very short trainset composed of an empty Fas E74 freight wagon (tare 24 t, fully loaded 80 t) hauled by an E190 Siemens Taurus locomotive was set up for the tests (Fig. 10).

The cylindrical pin of the supporting rod of a brake shoe holder was replaced with a modified one to install the device in the prescribed location. The rear of the measuring box was fixed to the bogie frame with an adjustable bracket (Fig. 11). The pyrometer and the slider inside the box were connected by elastic supports to limit the consequences of vertical and lateral shocks. The measuring chain was modified to be operated by using the 240-VAC sockets available on the locomotive. Cables for the pyrometer and the slideway were extended to both ends of the wagon allowing a fast connection with the other components located inside the locomotive.

Figure 12a–c shows three frames taken during the pyrometer movement starting from the flange side for a length of 80 mm. The outer part of the wheel tread is not of interest as it is in contact neither with the braking block nor with the rail and the useful run of the pyrometer is about 60 mm (Fig. 12a–b). As the axle guiding system of the Y25 bogie (Fig. 12d) has a lateral clearance $c = 10$ mm [28], the spot may fall outside the wheel surface when lateral movements of the wheelset occur. These events were captured and corrected during data processing.

4.2 Brake control

Normal braking is actuated by the locomotive driver acting on the brake valve managing the pressure in the UIC brake pipe [29]. To control the braking of the wagon independently from the locomotive, a fail-safe braking control device was added between the brake pipes of the wagon

 Springer

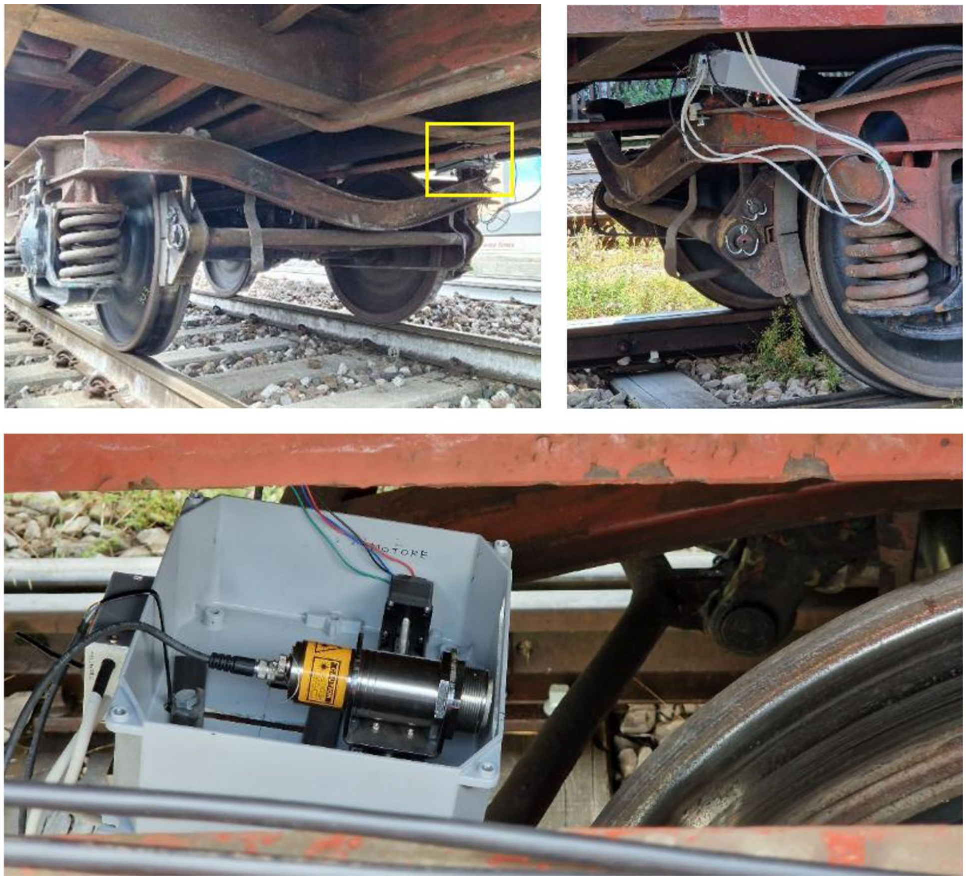

Fig. 11 The measuring box mounted on the Y25 bogie in front of the wheel surface

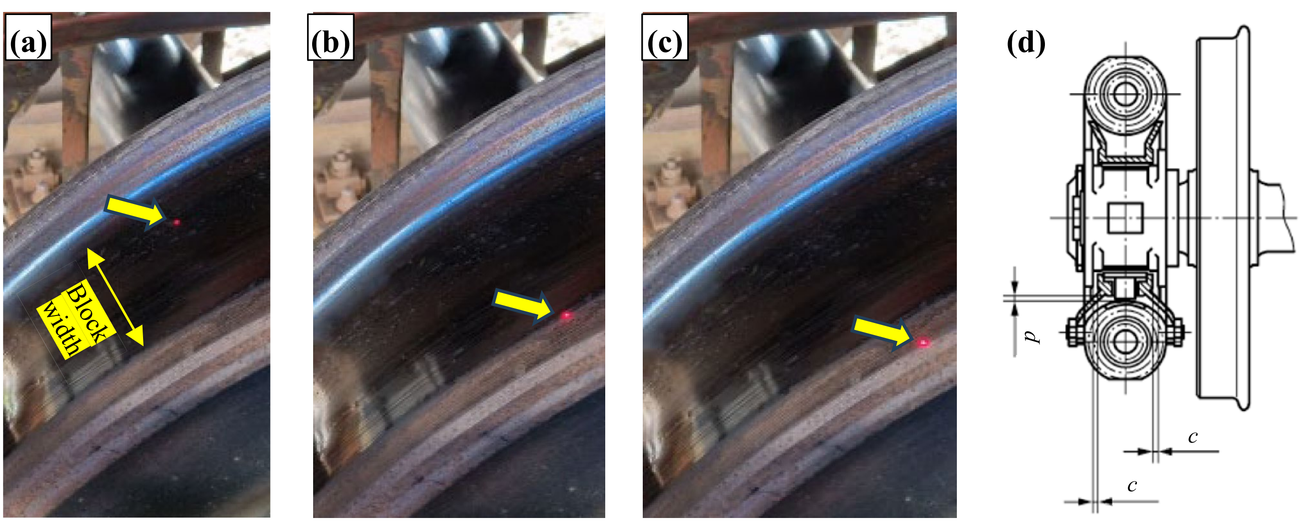

Fig. 12 **a–c** Sequence of the measuring spot positions from the inner to the outer portion of the wheel tread. **d** Lateral clearance c in the Y25 axlebox

and the locomotive (Fig. 13a). Additional valves (Fig. 13b) were placed inside the locomotive consisting in:

- a normally open monostable 3/2 valve with manual actuation used as shut-off valve,

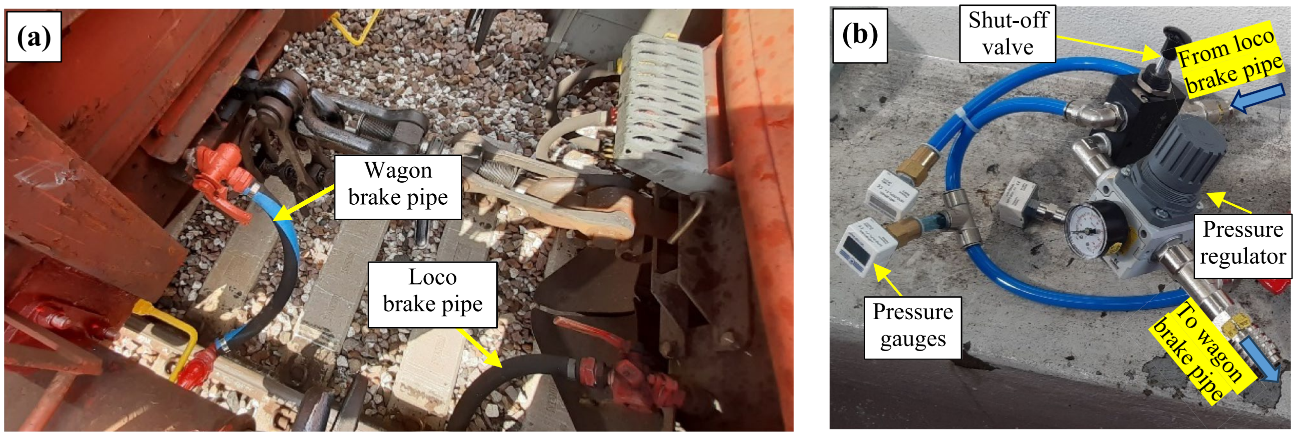

Fig. 13 **a** Brake pipes of the wagon and the locomotive intercepted by additional valves. **b** Valves used to control the wagon braking independently from the locomotive. Blue arrows indicate the airflow from the loco to the wagon

- a pressure regulator with manual actuation in parallel to the shut-off valve allowing to reduce the brake pipe pressure only on the wagon side.

In case of emergency, the release of the shut-off valve restores the continuity of the brake pipe between the locomotive and the wagon, while any lower brake pipe pressure commanded by the driver reaches the wagon distributor regardless of the pressure regulator position. The pressure values in the brake pipe on the locomotive side, on the wagon side, and in the brake cylinder of the wagon were monitored using digital pressure gauges.

When the brake pipe is shut (shut-off valve activated), the wagon braking force may be controlled by acting on the pressure regulator without affecting the locomotive that keeps hauling the wagon at constant speed being equipped with a speed regulator.

As Fas is a standardized wagon, the actual braking force arising from the brake cylinder pressure can be calculated according to UIC regulations [30] which include the relevant braking system scheme (Fig. 14a). Wagons are equipped with the *empty-loaded changeover device* (Fig. 14b) to adjust the braking force on the basis of the vehicle mass by a lever acting on the rigging distances between the brake cylinder and the brake blocks. Rigging distances and the relevant data for brake forces calculation in empty and loaded conditions are shown in Table 1.

To avoid undesired risks and possible major wheel damage due to excessive braking forces, applied when the total vehicle mass exceeds 40 t, tests were made in empty conditions. The braked mass in "empty" condition (28 t, see

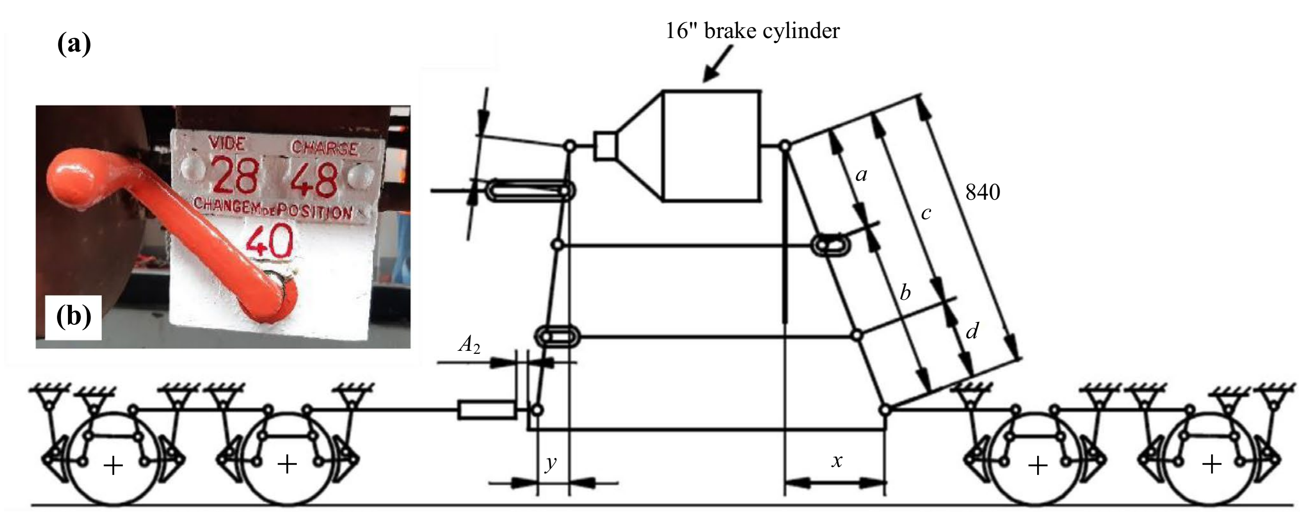

Fig. 14 **a** Scheme of the braking system of the Fas from [30]. **b** Photograph of the empty-loaded *changeover device* (unit: mm)

Table 1 Data of the braking system of the wagon with indication of the braking force in empty and loaded conditions from [30]

Parameter	Empty condition	Loaded condition
Brake rigging efficiency η	0.83	0.83
Opposing force from brake rigging adjuster F_R	2 kN	2 kN
Net force on piston F_t	47.71 kN	47.71 kN
Distances from ends of central brake rigging to pivot	$a=305$ mm $b=535$ mm	$c=500$ mm $d=340$ mm
Total multiplication ratio $i=8(a/b)$ or $8(c/d)$	4.56	11.76
Total force on brake blocks $F_{dyn}=(iF_t-8F_R)\eta$	167.32 kN	452.59 kN
Force on one brake block $F_n=F_{dyn}/16$	10.46 kN	28.29 kN
Value of coefficient k	1.662	1.126
Calculated braked weight $kF_{dyn}/9.81$	28 t	52 t

Fig. 14b) corresponds to a normal force $F_n=10.46$ kN on each brake block considering the full braking capacity, i.e., a pressure of 3.8 bar in the brake cylinder. Considering an average coefficient of friction for LL brake blocks of about $f=0.125$ [31], a maximum braking power of $P=fF_nV=58$ kW results at $v=80$ km/h. In "loaded" condition, the braking effort would have been 2.7 times higher.

The target brake cylinder pressure value and the resulting braking forces were not selected a priori but resulted from several braking attempts made at the beginning of the tests. The goal was to simulate a drag braking able to increase the wheel temperature over 350 °C without using the whole braking capacity of the wagon. The best compromise brake cylinder pressure was found to be about 2.3 bar, i.e., around 60% of the maximum pressure.

This braking condition does not correspond to normal service braking which unlikely would produce high temperatures, also considering that the line was almost flat and the wagon was empty. Braking was therefore artificially amplified to simulate more critical situations such as long and heavy train compositions, heavy drag braking on steep track, or in the worst-case failure of braking components (distributor valve or brake cylinder) that produce unduly continuous braking applications.

4.3 Test runs details

Tests were made on Udine-Treviso line, in the North of Italy, that is almost flat and straight with a few gentle curves for about 100 km, on September 11, 2025, with good weather conditions, scattered clouds, temperature nearly constant around 20–25 °C, no wind. Speed was maintained constant at 80 km/h speed, the lowest compatible with the other traffic present on the line, for most of the test run, even if some service stops occurred. The westbound run was used to make some preliminary checks on the system functionality while the eastbound (return) run was used to perform the desired tests.

Wagon braking was manually controlled using the shut-off manual valve and the pressure regulator, monitoring the pressure in the brake cylinder which was maintained as constant as possible in the range 2.0–2.5 bar during the whole

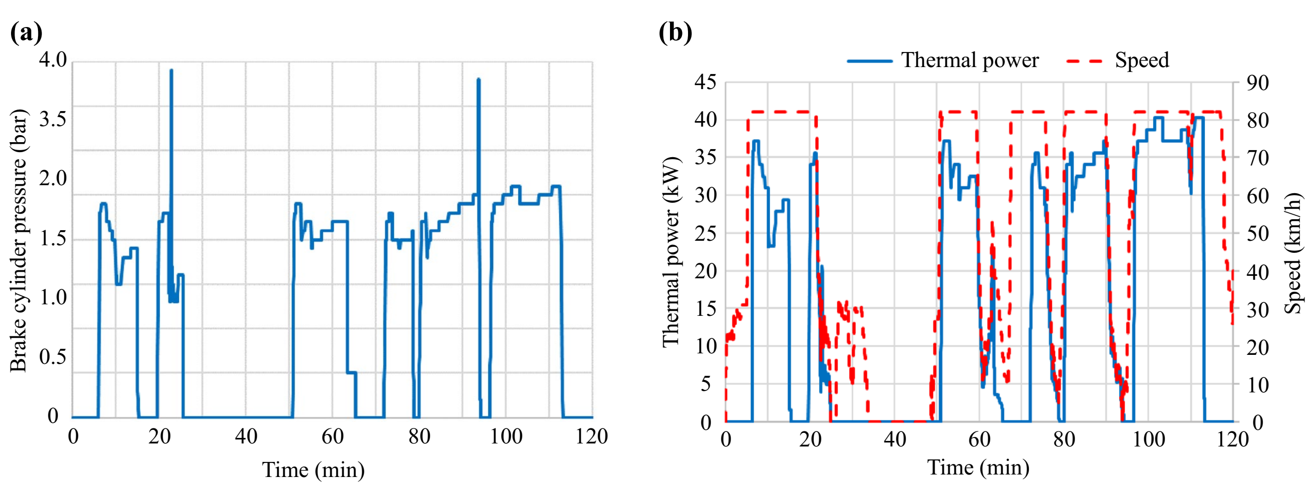

Fig. 15 **a** Pressure in the brake cylinder during the whole return run. **b** Speed of the train and calculated braking power during the return run

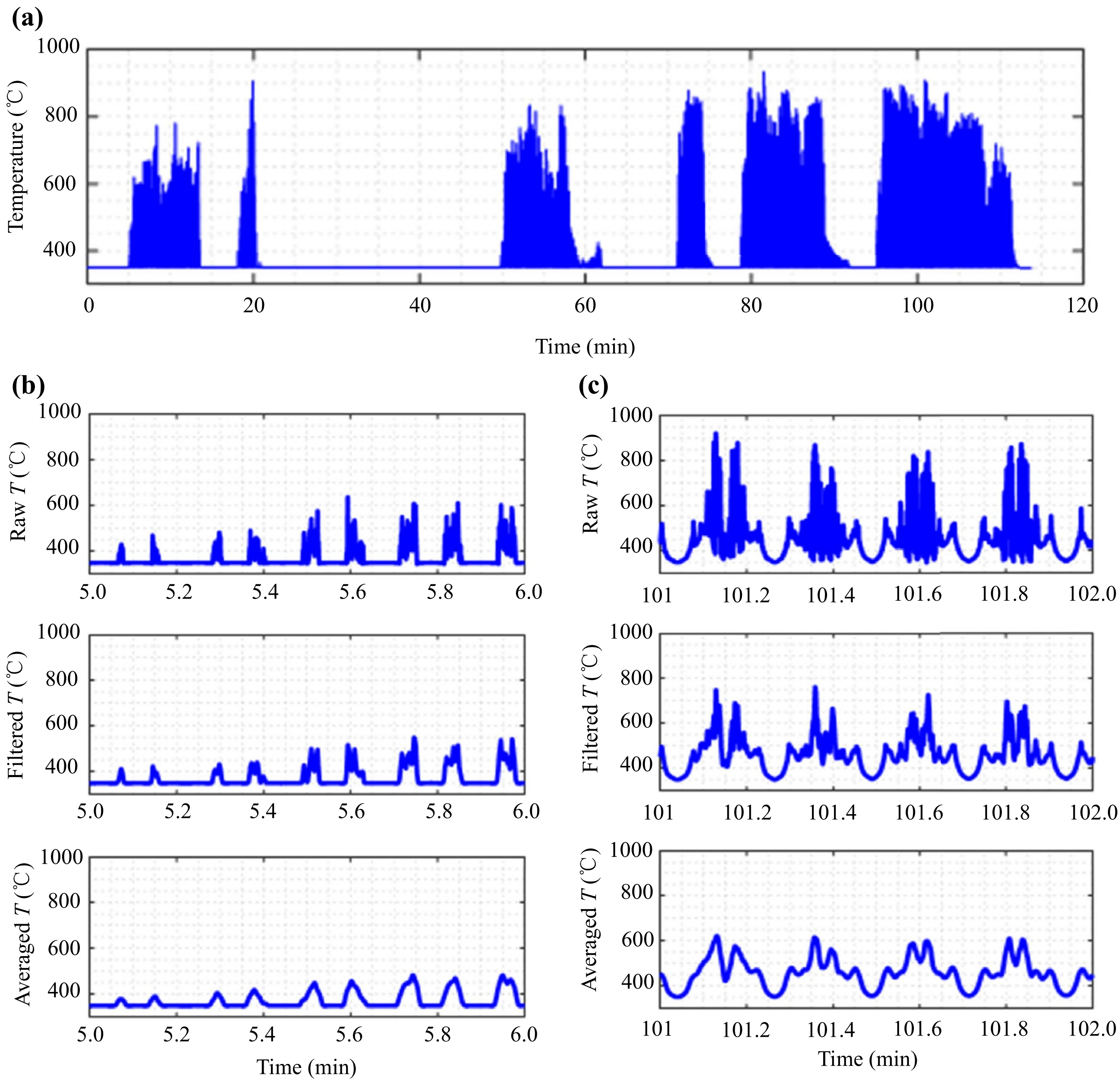

Fig. 16 Temperature recorded during the return run: **a** full length recording showing only raw temperature; **b** close-up of 1 min (t = 5–6 min) recording showing raw, filtered, and averaged data at the beginning of the run; **c** close-up of 1-min recording (t = 101–102 min) showing raw, filtered, and averaged data at the end of the run

eastbound return run. The pressure occasionally reached 3.8 bar when braking was applied by the driver (Fig. 15).

5 Discussion of the results

5.1 Data analysis

After about 4 h, the tests ended successfully without any issue, proving the robustness of the device. Temperature data were collected continuously during the eastbound return run with a sampling frequency of 100 Hz, then low-pass filtered at 10 Hz and subjected to a moving average process.

Raw data showed local peaks up to 900 °C (Fig. 16a), while processed data are obviously much smoother and less subject to local effects. It should be noted that this recording is related to the return run as the first run was used to adapt the brake block surface to freshly turned wheel profiles and to adjust the braking device operations, while during the return run, intense braking was applied since the beginning (as previously shown in Fig. 15).

Even if the starting temperature of the wheel is unknown, at the beginning of the return run cycles were mostly below 350 °C and only local peaks somewhere on wheel surface were recorded (Fig. 16b). Braking was maintained to heat the wheels up, and only in the last part of the run, the full pyrometer cycle was above 350 °C (Fig. 16c). The following may be concluded:

- Measurements are highly repeatable as the pyrometer cycles can be easily recognized.
- Temperature increases from the inner side (the point shown in Fig. 12a its the beginning of each cycle) to the outer side of the wheel profile.
- An excessive variability was found on the external side due to the combined effect of surface conditions and uncertain lateral position of the wheelset. Data were truncated to avoid considering these potentially corrupted data.

Due to the repeatability of the measuring cycles and the performed smoothing process, tread temperature can be considered constant along the circumference of the wheel, discarding the rotating and the scanning speed. A detailed analysis of the surface temperature for about 5 min ($t = 101$–106 min) of recording were therefore performed. In this interval, the braking conditions were quite stable and the temperature measured by the device was greater than 350 °C along the entire measuring cycle. In this time window, the smoothed temperatures were considered. Mirroring the back run of each pyrometer cycle, a total of 42 temperature profiles were obtained. Each point of these profiles corresponds to a specific axial position over the wheel tread.

The average local temperature and the standard deviation for each point on the surface are shown in Fig. 17a where they are compared to data acquired on the test bench

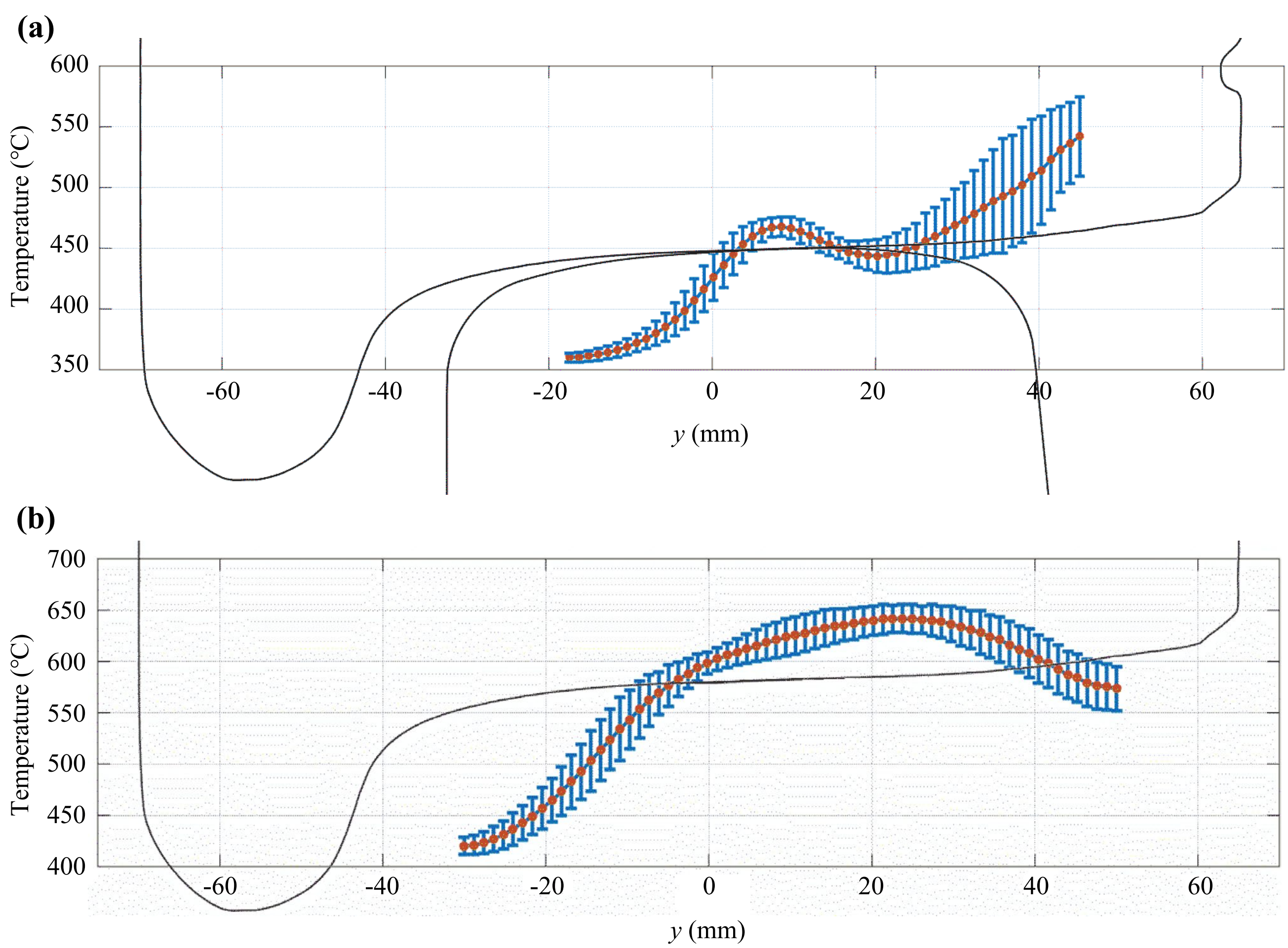

Fig. 17 Wheel tread surface temperature (average and standard deviation) for **a** in-service measurements and **b** bench test measurements (no rail present)

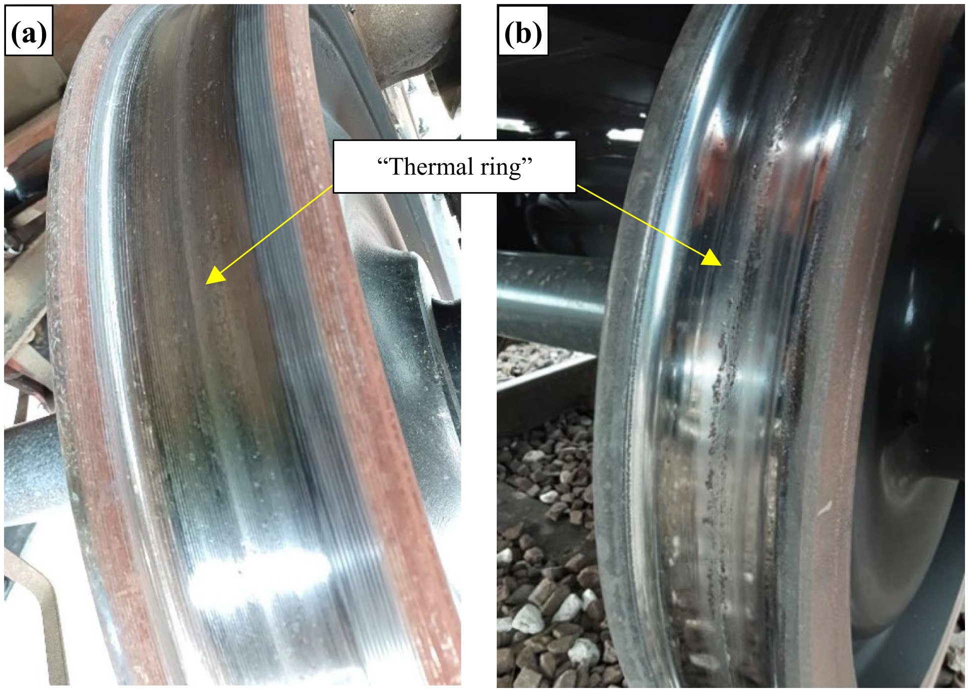

Fig. 18 Comparison of **a** the wheel surface after the braking tests and **b** the wheel surface with severe THRING damage [1]

(Fig. 17b). Data scatter is very small in the central part of the profile ($y = \pm 20$ mm); then, it increases on the outer part of the wheel tread. It is observed that the temperature does not increase linearly along the profile, showing a sort of stabilization in the central part of the surface where the wheel-rail contact is likely to occur. Authors cannot say if the surface found affected by the "thermal ring" phenomenon (see below) may have affected the emissivity of the surface. It can only be said that such surface looks silky at a naked eye, but nothing can be concluded about its radiation. In the following, it is assumed that such change, if present, may be neglected.

Data from bench tests, without the wheel–rail contact, do not show this behavior and the temperature profile is much more regular. Relevant differences between field tests and bench tests in terms of convective heat transfer on the wheel surface can be excluded as tests bench are designed with a forced airflow to simulate real running conditions. So, the different temperature distributions between field and bench may be related to a rail-chill effect even if it is not possible to quantify it as the braking conditions were much different.

All wheels showed signs of overheating (thermally sensitive paint cracks) at the end of the tests, confirming that high temperatures were reached. Surface damage was limited because of the low vertical load on the wheels (about 30 kN in empty conditions) and the short duration of the tests. Figure 18a shows the running surface of one of the wheels of the wagon used for the test in which signs of an incipient circumferential damage seems to be present when compared to a more developed thermal ring (THRING) damage [1] as shown in Fig. 18b. However, a detailed analysis of the wheel material is needed to evaluate the presence of subsurface cracks.

5.2 Future application of the device

The application of the presented device for extensive and long-term monitoring is out of the scope of this paper. However, it can be said that the device is not intended to replace wayside temperature monitoring currently installed along the line (HABD) or to be permanently mounted to the bogie frame. For example, it can be used together with other wayside measuring systems to find a correlation between tread temperature and side temperature of the wheel.

The device is intended to be used as an affordable additional system to the existing ones for the evaluation of brake blocks and wheels during the effective operating braking conditions of a freight wagons which cannot be fully reproduced on a test bench. Railway operators might use the device to evaluate and investigate braking components behavior and braking operating conditions as the certification of composite brake blocks performed with bench tests has shown severe limitations as proven by several in-service issues in the last years [1].

The device can be mounted on the bogie frame only when needed and dismounted easily. The number of devices to be installed should be carefully discussed considering that the actual braking force can be different between the wheels of the same wagon or the same bogie. Instrumented brake blocks [32] can be used before the test to verify the actual braking force on each wheel.

Duration of tests can be theoretically unlimited if the power supply is given by the locomotive, with limitations in terms of cabling and number of devices to be used, while long-lasting (several hours) unattended measurements can be reached using batteries due to the low-power consumption of the device. In this case, the device should be slightly modified to included more compact acquisition modules than a laptop.

6 Conclusions and prospects

The use of composite blocks to brake freight wagons reduced noise but increased tread damage compared to the cast iron brake blocks because of their lower thermal conductivity that introduced higher thermal loads in the wheel. The accurate, reliable, and affordable measurement of wheel tread temperature has therefore become a crucial factor to understand damage mechanisms largely unknown in the past.

A literature review has shown that no such devices exist, being most the tests made on test benches or at stationary locations during trains pass-by. Both these measurements have strong limitations as described in the paper.

The development and the calibration of a contactless measuring device designed with the aim to monitor the in-service temperature of wheel treads during braking was described. A moving infrared single-spot pyrometer working in the short wavelength range (1.5–1.8 µm) was selected as the best compromise between accuracy, compactness, and affordability.

The measuring chain was calibrated during braking sessions performed on a certified test rig by using cast iron brake blocks. As experimental data from sliding thermocouples resulted to be unreliable, only data only from embedded thermocouples were used as inputs of a three-dimensional thermal finite element model to estimate the surface temperature. These temperatures were then used according to radiation equations to adjust the emissivity in the pyrometer setting.

The improved prototype device was installed on a freight wagon, and measurements were performed during a specifically designed test campaign, providing data with good stability, reliability, and reproducibility.

Future activities will include metallurgical and mechanical tests on some wheels of the tested wagon as well as the repetition of the tests on other vehicles in similar and different conditions. To such goal, a small batch of improved devices in currently under development.

Acknowledgements InRail SpA, an Italian railway undertaking, is gratefully acknowledged for all the technical support provided during in-service tests.

References

1. Megna G, Bracciali A (2025) Tread-braked wheels: review and recent findings. Machines 13(7):579
2. Voortman Landström E, Vernersson T, Lundén R (2025) Characterisation and evaluation of global uneven heating during railway tread braking–Brake rig testing and field study. Proc Inst Mech Eng Part F J Rail Rapid Transit 239(3):258–271
3. Walia MS, Vernersson T, Lundén R et al (2019) Temperatures and wear at railway tread braking: field experiments and simulations. Wear 440–441:203086
4. Teimourimanesh S, Vernersson T, Lundén R et al (2014) Tread braking of railway wheels–temperatures generated by a metro train. Proc Inst Mech Eng Part F J Rail Rapid Transit 228(2):210–221
5. Vernersson T, Lundén R (2007) Temperatures at railway tread braking. Part 3: wheel and block temperatures and the influence of rail chill. Proc Inst Mech Eng Part F J Rail Rapid Transit 221(4):443–454
6. Orringer O, Gray DE (1995) Thermal cracking in railroad vehicle wheels subjected to high performance stop braking. Theor Appl Fract Mech 23(1):55–65
7. Vignoli M, Mazzoni S, Pampaloni T (1995) Influenza della frenatura dei treni sulla temperatura delle ruote. La Tec Prof 8:26–45
8. Cummings SM, Patil Dumbre SS (2023) Effects of braking on wheel wear and tread damage. In: Proceedings of the 12th international heavy haul association conference, Rio de Janeiro, 27–31 Aug 2023
9. Voestalpine, Infrared temperature measurement with zentrak. https://www.voestalpine.com/railway-systems/en/products/zentrak-hot-box-detection-and-hot-wheel-detection/. Accessed on Jan 8 2026
10. Parker RC, Marshall PR (1948) The measurement of the temperature of sliding surfaces, with particular reference to railway brake blocks. Proc Inst Mech Eng 158(1):209–229
11. International Union of Railways (1972) Semelles de frein en matériaux composites. ORE B64 - RP10, Utrecth
12. OPTRIS—Infrared Measurments. Non-contact temperature measurements metal industry. https://optris.com/wp-content/uploads/2024/10/Metal-BR-EN2023-05-B_web.pdf. Accessed on Mar 12 2026

13. Young HD, Freedman RA (2016) University physics with modern physics, 15th edn. Pearson, New York
14. Micro-epsilon. Basics of non-contact temperature measurements. https://www.micro-epsilon.in/fileadmin/download/products/dat--infrared-basics--en.pdf. Accessed on Jan 8 2026
15. Saunders P (2009) Calibration and use of low-temperature direct-reading radiation thermometers. Meas Sci Technol 20(2):025104
16. Hagqvist P, Sikström F, Christiansson A-K (2013) Emissivity estimation for high temperature radiation pyrometry on Ti–6Al–4V. Measurement 46(2):871–880
17. Keller. Two-colour pyrometers—principle, advantages, limitations and applications of two-colour pyrometers in thermal processes. https://www.pyrometer.com/reports/basics/two-colour-pyrometers/. Accessed on Jan 8 2026
18. Zhang J, Zuo J (2025) Numerical thermo-mechanical modeling of tread braking systems under ultra-long downhill constant-speed conditions with coupled time-dependent heat partition coefficients. Int Commun Heat Mass Transf 169:109713
19. Zhang R, Su L, Zhao C et al (2026) Experimental study on the relationship between freight train wheel brake temperature and slope gradient. Therm Sci Eng Prog 73:104644
20. Landström EV, Vernersson T, Lundén R (2023) Improved finite element modelling of tread braked wheel performance verified by brake rig tests. In: Proceedings of the 20th International Wheelset Congress (IWC), Chicago, 8–11 May 2023
21. Landström EV, Vernersson T, Lundén R (2024) Analysis and testing of tread braked railway wheel—effects of hot spots on wheel performance. Int J Fatigue 180:108116
22. Singh Walia M (2019) Mechanical braking systems for trains: a study of temperatures, fatigue and wear by experiments and simulations. Dissertation, Chalmers University of Technology
23. DIAS, PYROSPOT DS 40N and DG 40N - Pyrometer for industrial application. https://www.dias-infrared.de/pdf/pyrospot_ds40_dg40_eng.pdf. Accessed on Jan 8 2026
24. International Union of Railways (2006) Standardisation of wheelsets definition parameters for the thermomechanical calculation of wheels correlation between calculations and tests. UIC B169/RP 17
25. Faccoli M, Provezza L, Petrogalli C et al (2019) Effects of full-stops on shoe-braked railway wheel wear damage. Wear 428–429:64–475
26. Tran L, Cookson J, Chiu WK et al (2026) A review of thermal railway wheel modelling–applicability and limitations. Proc Inst Mech Eng Part F J Rail Rapid Transit 240(5):539–554
27. Esmaeili A, Walia MS, Handa K et al (2017) A methodology to predict thermomechanical cracking of railway wheel treads: from experiments to numerical predictions. Int J Fatigue 105:71–85
28. European Committee for Standardization (2023) Railway application—testing for the acceptance of running characteristics of railway vehicles—freight wagons—conditions for dispensation of freight wagons with defined characteristics from on-track tests according to EN 14363. EN 16235
29. International Union of Railways (2016) Brakes—air brakes for freight trains and passenger trains. UIC 540
30. International Union of Railways (2014) Brakes—braking performances. UIC 544–1
31. British Standards Institution (2015) Railway applications—braking—brake blocks. BS EN 16452:2015+A1:2019
32. Kistler. Brake force measuring system. https://assets.kistler.com.cn/SAPCommerce_Download_original/003-342e.pdf. Accessed 16 Mar 2026